Gadolinium Chelate Coated Gold Nanoparticles As Contrast Agents for Both X-ray Computed Tomography and Magnetic Resonance Imaging

ARTICLE *in* JOURNAL OF THE AMERICAN CHEMICAL SOCIETY · JUNE 2008

Impact Factor: 12.11 · DOI: 10.1021/ja078176p · Source: PubMed

12 AUTHORS, INCLUDING:

Christophe Alric
University of Tours
13 PUBLICATIONS **432** CITATIONS
SEE PROFILE

Claire Billotey
Université Jean Monnet
86 PUBLICATIONS **2,447** CITATIONS
SEE PROFILE

Marc F Janier
Claude Bernard University Lyon 1
139 PUBLICATIONS **2,406** CITATIONS
SEE PROFILE

Olivier Tillement
Claude Bernard University Lyon 1
277 PUBLICATIONS **3,799** CITATIONS
SEE PROFILE

J|A|C|S
ARTICLES

Published on Web 04/12/2008

Gadolinium Chelate Coated Gold Nanoparticles As Contrast Agents for Both X-ray Computed Tomography and Magnetic Resonance Imaging

Christophe Alric,[†] Jacqueline Taleb,[‡] Géraldine Le Duc,[§] Céline Mandon,[‡] Claire Billotey,[‡] Alice Le Meur-Herland,[‡] Thierry Brochard,[§] Francis Vocanson,[||] Marc Janier,[‡] Pascal Perriat,[⊥] Stéphane Roux,*[,†] and Olivier Tillement[†]

Laboratoire de Physico-Chimie des Matériaux Luminescents, UMR 5620 CNRS - Université Claude Bernard Lyon 1, 69622 Villeurbanne Cedex, France, Laboratoire CREATIS − Animage, UMR 5515 CNRS - U630 INSERM - INSA de Lyon - Université Claude Bernard Lyon 1, 69622 Villeurbanne Cedex, France, European Synchrotron Radiation Facility, ID 17 biomedical Beamline, Polygone Scientifique Louis Néel, 6 rue Jules Horowitz, 38000 Grenoble, France, Laboratoire Hubert Curien, UMR 5516 CNRS - Université Jean Monnet, 42000 Saint-Etienne, France, and Matériaux Ingénierie et Science, UMR 5510 CNRS - INSA de Lyon, 69621 Villeurbanne Cedex, France

Received October 25, 2007; E-mail: roux@pcml.univ-lyon1.fr

Abstract: Functionalized gold nanoparticles were applied as contrast agents for both in vivo X-ray and magnetic resonance imaging. These particles were obtained by encapsulating gold cores within a multilayered organic shell which is composed of gadolinium chelates bound to each other through disulfide bonds. The contrast enhancement in MRI stems from the presence of gadolinium ions which are entrapped in the organic shell, whereas the gold core provides a strong X-ray absorption. This study revealed that these particles suited for dual modality imaging freely circulate in the blood vessels without undesirable accumulation in the lungs, spleen, and liver.

Introduction

The achievement of preclinical studies in oncology which aim at developing and evaluating therapeutic strategies on models requires efficient new functionalized contrast agents for visualizing tumor growth, for monitoring the effect of a treatment and/or for inducing the destruction of cancerous tumors. Such applications imply adequate pharmacokinetic properties and low levels of nonspecific accumulation in the body. Recently many papers emphasize the development of nanoparticles as contrast agents for medical imaging since they have a longer vascular half-life than molecular contrast agents.[1–5] As a result, the particulate contrast agents can be monitored for a longer time after the delivery to a living organism. If a rapid elimination of the contrast agents is recommended for clinical diagnosis, their presence for a longer time can be useful for monitoring the biodistribution of drugs or radiosensitizing agents for cancer treatment and the response to a therapy in animal models. Another great advantage of the nanoparticles over the molecular contrast agents lies in their ability to gather in the same object several complementary properties. This attractive feature led to the development of multifunctional nanoparticles which can be detected by several in vivo imaging techniques.[6,7] Among the numerous possibilities, nanoparticles combining fluorescent imaging and magnetic resonance imaging (MRI) are probably the most frequently studied because they ally the high sensitivity of the fluorescence phenomenon to the high spatial resolution of MRI.[8–13] Although MRI has become a prominent noninvasive technique in diagnostic clinical

[†] Laboratoire de Physico-Chimie des Matériaux Luminescents, Université Claude Bernard Lyon 1.
[‡] Laboratoire CREATIS − Animage, INSA de Lyon - Université Claude Bernard Lyon 1.
[§] Polygone Scientifique Louis Néel.
[||] Université Jean Monnet.
[⊥] Matériaux Ingénierie et Science, INSA de Lyon.

(1) Ferrari, M. *Nat. Rev. Cancer* **2005**, *5*, 161–171.
(2) Brigger, I.; Dubernet, C.; Couvreur, P. *Adv. Drug Delivery Rev.* **2002**, *54*, 631–651.
(3) Sunderland, C. J.; Steiert, M.; Talmadge, E. J.; Derfus, M. A.; Barry, S. E. *Drug Dev. Res.* **2006**, *67*, 70–93.
(4) Yezhelyev, M. V.; Gao, X.; Xing, Y.; Al-Hajj, A.; Nie, S.; O'Reagan, M. R. *Lancet Oncol.* **2006**, *7*, 657–667.
(5) Gao, X.; Cui, Y.; Levenson, R. M.; Chung, L. W. K.; Nie, S. *Nat. Biotechnol.* **2004**, *22*, 969–976.
(6) Lewin, M.; Carlesso, N.; Tung, C. H.; Tang, X. W.; Cory, D.; Scadden, D. T.; Weissleder, R. *Nat. Biotechnol.* **2000**, *18*, 410–414.
(7) Torchilin, V. P. *Adv. Drug Deliv. Rev.* **2006**, *58*, 1532–1555.
(8) Bridot, J.-L.; Faure, A.-C.; Laurent, S.; Rivière, C.; Billotey, C.; Hiba, B.; Janier, M.; Josserand, V.; Coll, J.-L.; Vander Elst, L.; Muller, R.; Roux, S.; Perriat, P.; Tillement, O. *J. Am. Chem. Soc.* **2007**, *129*, 5076–5084.
(9) Mulder, W. J. M.; Koole, R.; Brandwijk, R. J.; Storm, G.; Chin, P. T. K.; Strijkers, G. J.; de Mello Donega, C.; Nicolay, K.; Griffioen, A. W. *Nano Lett.* **2006**, *6*, 1–6.
(10) van Tilborg, G. A. F.; Mulder, W. J. M.; Chin, P. T. K.; Storm, G.; Reutelingsperger, C. P.; Nicolay, K.; Strijkers, G. J. *Bioconjugate Chem.* **2006**, *17*, 865–868.
(11) Medarova, Z.; Pham, W.; Kim, Y.; Dai, G.; Moore, A. *Int. J. Cancer* **2006**, *118*, 2796–2802.
(12) Veiseh, O.; Sun, C.; Gunn, J.; Kohler, N.; Gabikian, P.; Lee, D.; Bhattarai, N.; Ellenbogen, R.; Sze, R.; Hallahan, A.; Olson, J.; Zhang, M. *Nano Lett.* **2005**, *5*, 1003–1008.
(13) Bertorelle, F.; Wilhelm, C.; Roger, J.; Gazeau, F.; Ménager, C.; Cabuil, V. *Langmuir* **2006**, *22*, 5385–5391.

 10.1021/ja078176p CCC: $40.75

medicine owing to the possibility of obtaining highly resolved three-dimensional images of living bodies, the in vivo application of these fluorescent MRI contrast agents is limited to small animal imaging because of the autofluorescence, the strong light absorption, and scattering which limit the spatial resolution.[4,5,14] On the contrary, X-ray computed tomography (CT) imaging is widely used for diagnosis since X-rays can go across the human body.[15] The internal anatomic structures can therefore be externally visualized without surgery. However the administration of contrast agents can be required. Iodinated molecules[16,17] are applied daily as contrast agents for CT imaging due to the high X-ray absorption coefficient of iodine and their innocuousness (except in a few cases of patients with poor kidney function), but their rapid pharmacokinetics and the high viscosity of the injectable solution can however constitute a handicap.[18] Despite the ubiquitous nature of CT in clinical settings, the development of nanoparticles as contrast agents for CT received little attention although they can induce greater contrast enhancement of CT images than iodinated compounds. Moreover nanoparticles are distinguished by their multifunctionality which is the key advantage over traditional approaches since it allows combining several imaging techniques or imaging and therapy. The use of dense nanoparticles containing high atomic number elements as contrast agents for X-ray CT imaging was recently proposed. Gold nanoparticles were efficiently applied in vivo as X-ray contrast agents.[19] As expected, these particles induce, for the same content of absorbing element, a higher contrast than iodinated compounds. This ability seems independent of the diameter of gold nanoparticles because similar contrast enhancement is observed for both 1.9 and 31 nm sized particles.[19–21] If no data about the surface chemical composition of the smallest particles are available, the biggest ones were coated by thiolated PEG which provides a long plasma circulation time. Even if quantum dots[22] and bismuth sulfide[23] nanoparticles exhibit the ability to enhance the contrast of CT images which is in the case of Bi_2S_3 stronger than iodinated compounds, gold nanoparticles are more attractive candidates since it is easier to control the size, the shape, and the surface chemical composition of gold nanoparticles.[24] The facile derivatization of gold nanoparticles is crucial for developing new tools for biomedical application which meet the criteria of clinical use.[25] We recently demonstrated that gold nanoparticles functionalized by gadolinium chelates are able to induce in vitro positive contrast in the MR images.[26] Such particles appear therefore very attractive because they could behave as contrast agents for both X-ray imaging and MRI.

In this paper we report on the results of the in vivo application of gadolinium chelate coated gold nanoparticles. After intravenous injection to mice and rats, the biodistribution of these nanoparticles was monitored by MRI (at 7T) and X-ray imaging which was performed at the biomedical beamline of the European Synchrotron Radiation Facility (ESRF). This biomedical line affords attractive conditions for computed tomography (SRCT for Synchrotron Radiation Computed Tomography) because synchrotron radiation provides monochromatic X-ray beams whose intensity is 5 orders of magnitude higher than the one provided by conventional X-ray sources. Unlike the conventional scanners which are handicapped by intensity variations, limited flux, and broad energy spectrum, SRCT allows quantifying the contrast agent concentration in the tissues. The nondestructive and absolute quantitative in vivo measurement of gold concentration constitutes an original and attractive feature of monochromatic X-ray beams for monitoring in "real time" the biodistribution of gold nanoparticles, since it does not require the sacrifice of the animal in contrast to the postmortem ICP analyses.

Experimental Section

Chemicals. Diethylenetriaminepentacetic acid bis-anhydride (DTPA-BA), tetrachloroauric acid trihydrate ($HAuCl_4 \cdot 3H_2O$), sodium borohydride ($NaBH_4$), acetic acid (CH_3COOH), aminoethanethiol, and sodium hydroxide (NaOH) were purchased from Aldrich. Methanol, dimethylformamide (DMF), triethylamine, and other organic solvents (reagent grade) were purchased from SDS and used as received. For the preparation of an aqueous solution and for the rinsing of gold nanoparticles, only milli-Q water ($\rho <$ 18 MΩ) was used. The filtration of gold nanoparticles was performed on a polymer membrane of 0.22 μm pore diameter purchased from Osmonics Inc.

DTDTPA Synthesis. In a round flask of 250 mL, 2 g (5.6×10^{-3} mol) of diethylenetriaminepentacetic acid bis-anhydride were dissolved in 40 mL of dimethylformamide and then heated to 70 °C. In an other flask, 1.1 g (1.43×10^{-2} mol) of aminoethanethiol was dissolved in 30 mL of DMF and 1.74 mL of triethylamine. This solution was added to the round flask and was stirred magnetically at 70 °C overnight. Then, the solution was first cooled to room temperature and then was put in an ice bath. A white powder (NEt_3,HCl) precipitated and was filtered. The filtrate was concentrated at low pressure. After addition of this solution to a chloroform solution, a white precipitate was formed. After filtration of solution, washing with 50 mL of chloroform and drying under vacuum, DTDTPA was obtained as a white powder (90% yield).

^{1}H NMR (300 MHz, D_2O, 298 K): δ 3.81 (s, 4H, $-N-CH_2-CO-N-$), 3.69 (s, 4H, $-N-CH_2-COOH$), 3.64 (s, 2H, $-N-CH_2-COOH$), 3.38–3.20 (m, 12H, $-N-CH_2-CH_2-SH$, $-N-CH_2-CH_2-N$), 2.59 (t, 4H, $N-CH_2-CH_2-SH$). ^{13}C NMR (75 MHz, D_2O, 298 K): δ: 172.48 and 172.18 ($-N-CH_2-COOH$), 168.93 ($-N-CH_2-CO-N$), 57.17 and 56.86 ($-N-CH_2-COOH$), 54.76 ($N-CH_2-CO-N$), 52.17 and 51.55 ($-N-CH_2-CH_2-N-$), 42.61 ($-N-CH_2-CH_2-SH$), 23.68 ($-N-CH_2-CH_2-SH$). IR: 2929 (ν CH-alkyl), 2530 (ν SH), 1718 (ν CO,COOH), 1646 (ν CO, RCONR′R″), 1533 (ν CO, RCONHR′) cm^{-1}. The comparison of spectra of DTPA and DTDTPA shows clearly the emergence of a characteristic S−H (ν) band at 2530 cm^{-1}. ES-MS (+): m/z = 512 ($[M + H]^+$); 534.2 ($[M + Na]^+$).

(14) Medintz, I. L.; Uyeda, H. T.; Goldman, E. R.; Mattoussi, H. *Nat. Mater.* **2005**, *4*, 435–446.
(15) Yu, S.-B.; Watson, A. D. *Chem. Rev.* **1999**, *99*, 2353–2377.
(16) Idée, J.-M.; Nachman, I.; Port, M.; Petta, M.; Le Lem, G.; Le Greneur, S.; Dencausse, A.; Meyer, D.; Corot, C. *Top. Curr. Chem.* **2002**, *222*, 151–171.
(17) Krause, W.; Schneider, P. W. *Top. Curr. Chem.* **2002**, *222*, 107–150.
(18) McClennan, B. L. *Invest. Radiol.* **1994**, *29*, S46–S50.
(19) Hainfeld, J. F.; Slatkin, D. N.; Focella, T. M.; Smilowitz, H. M. *Brit. J. Radiol.* **2006**, *79*, 248–253.
(20) Kim, D.; Park, S.; Lee, J. H.; Jeong, Y. Y.; Jon, S. *J. Am. Chem. Soc.* **2007**, *129*, 7661–7665.
(21) Kattumuri, V.; Katti, K.; Bhaskaran, S.; Boote, E. J.; Casteel, S. W.; Fent, G. M.; Roberston, D. J.; Chandrasekhar, M.; Kannan, R.; Katti, K. *Small* **2007**, *3*, 333–341.
(22) Santra, S.; Yang, H.; Holloway, P. H.; Stanley, J. T.; Mericle, R. A. *J. Am. Chem. Soc.* **2005**, *127*, 1656–1657.
(23) Rabin, O.; Perez, J. M.; Grimm, J.; Wojtkiewicz, G.; Weissleder, R. *Nat. Mater.* **2006**, *5*, 118–122.
(24) Daniel, M.-C.; Astruc, D. *Chem. Rev.* **2004**, *104*, 293–346.
(25) Lewinski, N.; Colvin, V.; Drezek, R. *Small* **2008**, *4*, 26–49.
(26) Debouttière, P.-J.; Roux, S.; Vocanson, F.; Billotey, C.; Beuf, O.; Favre-Réguillon, A.; Lin, Y.; Pellet-Rostaing, S.; Lamartine, R.; Perriat, P.; Tillement, O. *Adv. Funct. Mater.* **2006**, *16*, 2330–2339.

Functionalized Gold Nanoparticles Preparation. The synthesis, described by Brust et al., consists of reducing $HAuCl_4 \cdot 3H_2O$ with $NaBH_4$ in the presence of thiols (stabilizers) which, by adsorption on growing particles, ensures control of the size and the stability of the colloid.[27]

For a typical preparation of gold particles, 200 mg (51×10^{-5} mol) of $HAuCl_4 \cdot 3H_2O$, dissolved in 60 mL of methanol, were placed in a 250 mL round-bottom flask. 256 mg (50×10^{-5} mol) of DTDTPA in 40 mL of water and 2 mL of acetic acid were added to the gold salt solution under stirring. The mixture turned from yellow to orange. After 5 min, 185 mg (489×10^{-5} mol) of $NaBH_4$ dissolved in 14 mL of water were added to the orange mixture under vigorous stirring at room temperature. At the beginning of the $NaBH_4$ addition, the solution became first dark brown then a black flocculate appeared.

The vigorous stirring was maintained for 1 h before adding 5 mL of 1 M aqueous hydrochloric acid solution. After the partial removal of the solvent under reduced pressure and at a maximum of 40 °C, the precipitate was filtered on a polymer membrane and washed thoroughly and successively with 0.01 N HCl, water, and diethyl ether. The resulting black powder (Au@DTDTPA) was dried and stocked in the solid state or dispersed in 10 mL of 0.01 M NaOH solution (up to 200 mg of dry powder).

Complexation of Gd^{3+} with Au@DTDTPA. Gd^{3+} complexation is carried out through the addition of $GdCl_3$ to the Au@DTDTPA colloidal solution under stirring at room temperature. The quantity of Gd^{3+} is monitored by colorimetric titration with xylenol. The mass ratio can also slightly vary depending on the nanoparticles synthesis, but for a typical solution of 60 mg of Au@DTDTPA, 2.0×10^{-5} mol of $GdCl_3$ are added.

NMR, FT-IR, and Mass Spectrometry Experiments. ^1H and ^{13}C NMR spectra were recorded using a Bruker AM 300 spectrometer. FT-IR spectra were recorded on a Perkin Spectrum One spectrometer. Mass spectra were obtained by an electrospray technique on an API 165 PE SCIEX engine.

UV–visible Spectroscopy Studies. UV–visible absorption spectra were recorded at room temperature with a Shimadzu UV-2401 PC spectrophotometer for measuring the absorption band of functionalized gold nanoparticles in the 400–800 nm range. The spectral measurements were performed on a diluted colloid dispersion of approximately 0.2 $g \cdot L^{-1}$ introduced in a standard quartz cuvette.

Colorimetric Titration of DTDTPA on Nanoparticles. The presence and the amount of free Gd^{3+} ions (i.e., Gd^{3+} ions which were not complexed by DTDTPA) have been determined by a colorimetric titration with xylenol orange (a weaker lanthanide chelating agent than DTDTPA). The titration was performed by the successive addition of an aqueous $GdCl_3$ (3.9 mM) solution to the Au@DTDTPA colloid. After each addition a small aliquot was taken and introduced into a xylenol orange solution whose pH was adjusted between 2 and 4 to put xylenol in the optimal conditions for observing the color change induced by the complexation of Gd^{3+}. The titration was monitored by UV–visible spectrophotometry and compared to the titration of a negative control (water or DTDTPA solution, i.e., in both cases in the absence of gold particles). This kind of titration indirectly indicates the number of Gd^{3+} which was chelated and hence the number of ligands anchored onto the particles.

High Resolution Transmission Electron Microscopy. HRTEM was used to obtain detailed structural and morphological information about the samples and was carried out using a JEOL 2010 microscope operating at 200 kV. The samples for HRTEM were prepared by depositing a drop of a diluted Au@DTDTPA colloidal solution on a carbon grid and allowing the liquid to dry in air at room temperature.

T_1 Measurements and MR Imaging. T_1 measurements and MR imaging were performed at 7T using an inversion–recovery FLASH (IR-FLASH) imaging sequence with varying IR time (Biospec System 70/20, Brucker, Ettlingen, Germany). T_1-weighted contrast enhancement was controlled running a standard Spin–Echo (SE) sequence with 500 ms TR and 12 ms TE. For in vivo imaging, anesthesia was induced with 1.8–2% isoflurane and maintained with 1.4–1.6% isoflurane in a mixture of O_2/N_2 (25/75%).

ζ-Potential Measurements. Direct determination of the ζ-potential of the Au@DTDTPA nanoparticles was performed via a Zetasizer NanoS (laser He−Ne (633 nm)) from Malvern Instrument. Prior to the experiment, the sol was diluted to obtain a concentration of ~ 0.08 $g \cdot L^{-1}$ in an aqueous solution containing 0.01 M NaCl and adjusted to the desired pH.

SRCT Imaging. SRCT images of phantoms containing Au@DTDTPA at various gold concentrations and in vivo imaging were performed via the biomedical beamline ID17 from the European Synchrotron Radiation Facility (Grenoble, France). The SRCT images were obtained by positioning the center of the sample at the convergence point of two beams bracketing the gold K edge energy (80.7 keV). After they crossed at the center of the sample (they can be considered as superimposed over the whole sample width), these beams diverged to match two distinct lines on the detector, allowing the simultaneous acquisition of attenuation profiles at 80.5 and 80.9 keV (below and above the gold K-edge, respectively). From the logarithmic subtraction of the attenuation profiles acquired simultaneously at two energies above and below the gold K-edge, accurate absolute gold concentrations can be determined. This method has been described elsewhere.[28,29] The injections and the imaging experiments were carried out on rats which were anesthetized by intraperitoneal injection of a mixture of xylazine/ketamine.

Inductively Coupled Plasma-Mass Spectrometry (ICP-MS) Analysis. Determination of gold content in organs was performed by ICP-MS analysis (Agilent 7500ce). Organs are dissolved in aqua regia. The resulting solutions were diluted in HNO_3 (2%, 2 ppb In, 1:300 v/v for brain, heart, spleen, and lungs and 1:3000 v/v for liver and kidneys).

Results and Discussion

The gadolinium chelate coated gold nanoparticles (Au@DTDTPA-Gd) were synthesized by reducing a gold salt ($HAuCl_4 \cdot 3H_2O$) with sodium borohydride ($NaBH_4$) in the presence of dithiolated derivatives of diethylenetriaminepentaacetic acid (DTDTPA) (Scheme 1).

In addition, to control the particle's growth and to avoid the agglomeration as expected in the case of a synthesis based on the protocol published by Brust and his co-workers,[27] these ligands play two other crucial roles, as shown in a previous paper.[26] Since bis-amide derivatives of DTPA are proven to be strong ligands for chelating the gadolinium ion (Gd^{3+}) even if the stability constant of these complexes (10^{16}–10^{18}) is weaker than the one of DTPA-Gd ($\sim 10^{22.5}$) which is widely used as MRI contrast agents for clinical diagnosis, the DTDTPA shell on the particles will allow the immobilization of Gd^{3+}. Moreover the presence of two thiol groups in DTDTPA led to the formation of a robust multilayered ligand shell. In contrast to other dithiolated ligands that are firmly anchored on the gold particle surface by both thiolate ends,[30–32] some DTDTPAs of

(27) Brust, M.; Fink, J.; Bethell, D.; Schiffrin, D. J.; Kiely, C. *J. Chem. Soc., Chem. Commun.* **1995**, 1655–1656.

(28) Adam, J.-F.; Nemoz, C.; Bravin, A.; Fielder, S.; Bayat, S.; Monfraix, S.; Berruyer, G.; Charvet, A.-M.; Le Bas, J.-F.; Elleaume, H.; Estève, F. *J. Cereb. Blood Flow Metab.* **2005**, *25*, 145–153.

(29) Elleaume, H., et al. *Nucl. Inst. Meth. Phys. Res. A* **1999**, *428*, 513–527.

(30) Garcia, B.; Salomé, M.; Lemelle, L.; Bridot, J.-L.; Gillet, P.; Perriat, P.; Roux, S.; Tillement, O. *Chem. Commun.* **2005**, 369–371.

(31) Roux, S.; Garcia, B.; Bridot, J.-L.; Salomé, M.; Marquette, C.; Lemelle, L.; Gillet, P.; Blum, L.; Perriat, P.; Tillement, O. *Langmuir* **2005**, *21*, 2526–2536.

Scheme 1. Synthesis of Au@DTDTPA-Gd Nanoparticles (Red Circle = Gd^{3+} Ion)

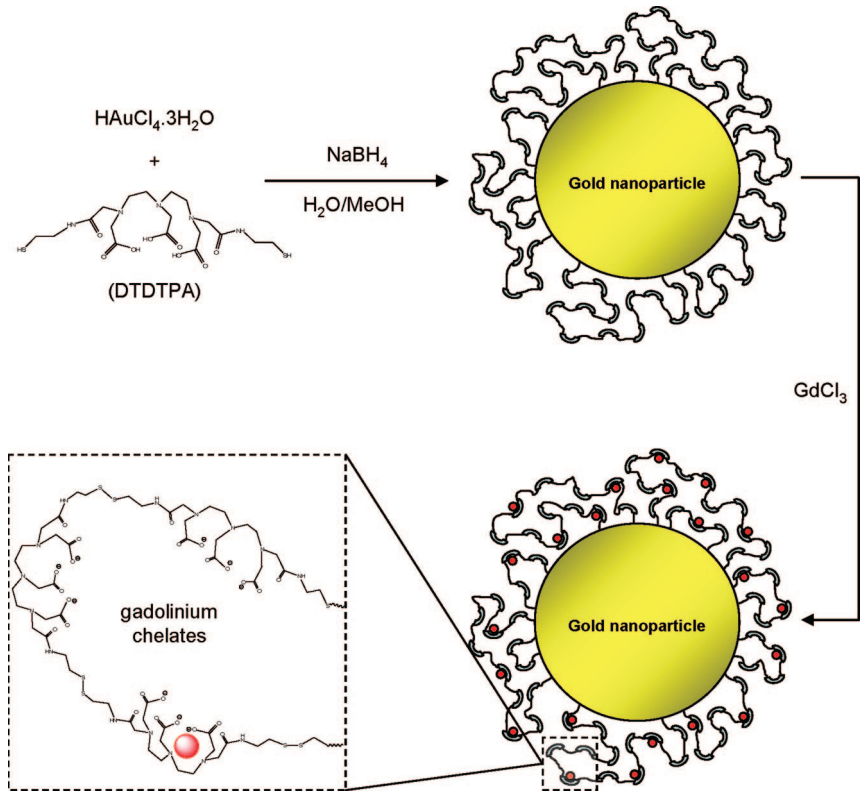

the organic shell are tethered to the surface by only one thiol group. But it was demonstrated in a previous paper that the thiol moieties which do not interact with gold atoms establish disulfide bonds between neighboring DTDTPAs.[26] As a result, for gold to $NaBH_4$ and gold to DTDTPA molar ratios of 0.104 and 1.020, respectively, 2.4 nm sized gold nanoparticles with a narrow size distribution are embedded in an organic shell composed of ~150 DTDTPA (Figure 1a). The number of DTDTPA on gold nanoparticles was indirectly determined by a colorimetric titration based on a competitive complexation of gadolinium by the DTDTPA shell and xylenol orange (a weaker ligand than DTDTPA) since the coordination of xylenol orange to Gd^{3+} is accompanied by a drastic modification of UV–visible absorption spectra which is reflected by a color change from yellow to pink. The color change of xylenol orange is observed when a gadolinium amount larger than 157 Gd^{3+} per particle was added to the colloidal solution. On the other hand, the absorption spectrum exhibits two bands around 479 and 569 nm (Figure 1b, blue curve), whereas the absorption spectrum of free xylenol orange has only a single peak centered around 443 nm (Figure 1b, black curve). The spectral modification and the color change indicate that xylenol orange is coordinated to the gadolinium ion. This is possible only if there is no available DTDTPA left since Gd^{3+} is preferentially chelated by DTDTPA. From these data we can deduce that about 150 gadolinium ions per particle can be immobilized on the particles. In other words, the organic shell is composed of at least 150 DTDTPA molecules. This was confirmed by TGA analysis.[26]

However the incorporation of 150 gadolinium ions per particle seriously alters the colloidal stability for gold content >1 $g \cdot L^{-1}$ since the positive charges of Gd^{3+} compensate the negative charges of the organic shell. Agglomerates appear after a day, whereas in absence of Gd^{3+} ions in the organic shell the colloid is stable for several weeks over a broad pH range (from 2 to 14) due to the electrostatic repulsion. This lack of stability which can impede the use of these particles as contrast agents for in vivo applications is overcome if the amount of gadolinium was limited to ~50 per particle (i.e., Gd to DTDTPA molar ratio: 0.33). As expected, all the gadolinium ions are entrapped in the DTDTPA shell since the absorption spectrum of xylenol orange in the presence of Au@DTDTPA-Gd_{50} is very similar to the spectrum of xylenol orange in the absence of gadolinium ions (Figure 1b, red curve). Although the zeta potential of Au@DTDTPA-Gd_{50} (−25 mV at pH 7.4 with 0.01 M NaCl) is smaller than the one of Au@DTDTPA (−32 mV at pH 7.4 with 0.01 M NaCl), the negative charge is sufficiently strong to ensure a colloidal stability (gold content: 10 $g \cdot L^{-1}$) in a physiological medium (pH 7.4, 150 mM NaCl) for at least a week and to envisage their use for in vivo application.

Prior to in vivo imaging studies, X-ray absorption and MRI experiments were carried out with aqueous solutions containing various concentrations of gold and gadolinium. SRCT images of phantoms containing Au@DTDTPA at various gold concentrations (from 0.14 to 10 $mg \cdot mL^{-1}$, i.e., $0.71 \leq [Au] \leq 50.7$ mM) and Au@DTDTPA-Gd_{50} (5.6 $mg \cdot mL^{-1}$, i.e., [Au] = 28.4 mM) show obviously that these particles induce a contrast enhancement when the gold concentration is at least equal to 1.4 $mg \cdot mL^{-1}$ (Figure 2).

As expected, the detection threshold is higher when CT images were acquired on a conventional CT scanner (Figure S1 in the Supporting Information). The analysis of CT data, by using the Hounsfield units (HU) for regions of interest, revealed that 50.7 mM Au@DTDTPA nanoparticles (10 g of Au L^{-1}) gives an equivalent X-ray absorption (1287 HU vs 1298 HU)

(32) Li, Z.; Jin, R.; Mirkin, C. A.; Letsinger, R. L. *Nucleic Acids Res.* **2002**, *30*, 1558–1562.

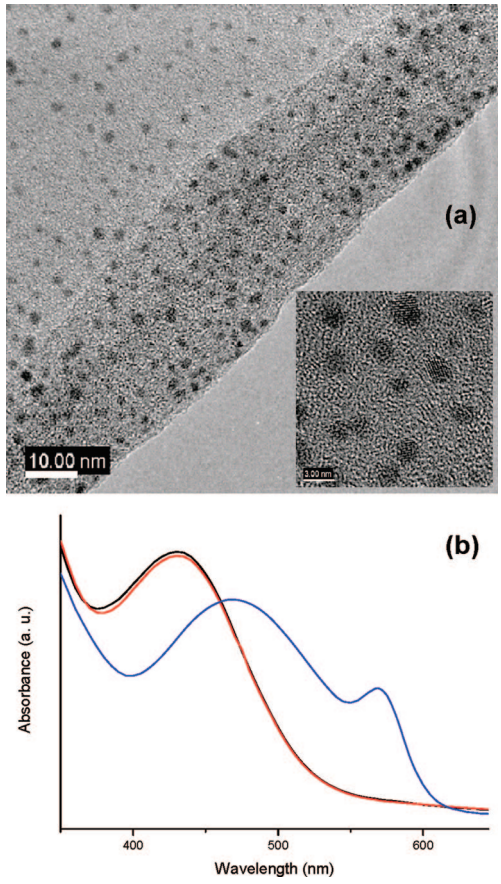

Figure 1. (a) Transmission electron micrograph of Au@DTDTPA nanoparticles. Inset: high resolution TEM of Au@DTDTPA nanoparticles. (b) UV–vis spectra of a solution of xylenol orange in the presence of Au@ DTDTPA-Gd_x nanoparticles with $x = 0$ (black curve), 50 (red curve), and >157 (blue curve).

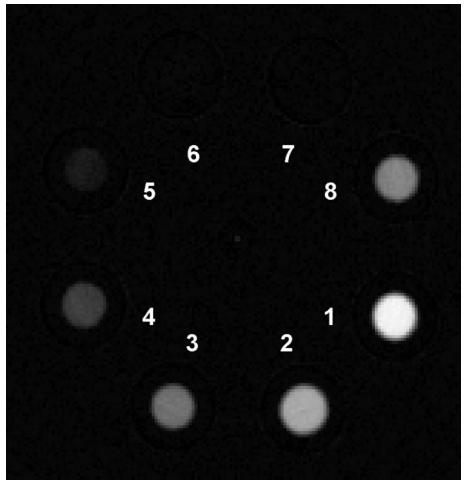

Figure 2. SRCT images of phantoms containing various Au@DTDTPA nanoparticles concentrations (1–7, see Table 1 for the gold concentration values) and Au@DTDTPA-Gd_{50} (8).

as 280 mM iodine (35 mg of I mL^{-1}). Besides a better sensitivity, SRCT experiments allow also the determination of gold concentration (Table 1). Except the case of the phantoms 6 and 7 which contain the lowest amount of gold (0.56 and 0.14 mg·mL^{-1}, respectively), the calculated concentrations are in accordance with the expected values (i.e., the weight of gold nanoparticles powder dispersed in a given volume). However the values determined from slices of each phantom are slightly smaller than the expected gold concentration. This difference can be attributed to the uncertainties inherent in the preparation of the colloidal solution.

This gap is smaller for sample 8 which is prepared from Au@DTDTPA-Gd_{50}. Although the gadolinium K-edge energy (50.2 keV) is largely lower than the one of gold, gadolinium ions immobilized on each nanoparticle ([Gd] = 2.5 mM for [Au] = 28.4 mM) seem to contribute to a small contrast enhancement of the SRCT images. But the main role of Gd^{3+} aims at increasing the positive contrast of the MR images. Since a colloid with a gold concentration of 10 mg·mL^{-1} provides the highest contrast for SRCT images, the influence of Au@ DTDTPA-Gd_x on the longitudinal relaxation time (T_1) was investigated with the same gold concentration at 25 °C. Relaxation time measurements and MR imaging were carried out at 7 T using an inversion–recovery FLASH (IR-FLASH) imaging sequence with varying IR time (Biospec System 70/ 20, Brucker, Ettlingen, Germany). T_1-weighted contrast enhancement was performed running a standard spin echo (SE) sequence with 500 ms TR and 12 ms TE. T_1-weighted images of phantoms containing aqueous colloids of Au@DTDTPA-Gd_x nanoparticles (with gold concentration: 10 mg·mL^{-1} and x, the number of Gd^{3+} ions per particle, varying from 0 to 50) confirm that these particles behave as positive contrast agents: the phantoms appear brighter than the negative controls (i.e., water and Au@DTDTPA) (Figure 3a). The phantom containing Au@$DTDTPA_{20}$ ([Gd] = 2 mM) appears the brightest even if there are two samples richer in gadolinium ions (Au@ $DTDTPA_{40}$ ([Gd] = 4 mM) and Au@$DTDTPA_{50}$ ([Gd] = 5 mM)). This observation is corroborated by the shape of the graph $1/T_1$ as a function of [Gd] (Figure 3b) since a plateau after a linear part until [Gd] = 2 mM appears. This plateau is the sign of T_2* effect and T_1-saturation at >2 mM Gd.[33]

Moreover the longitudinal relaxivity r_1 (the slope of the graph $1/T_1$ as a function of [Gd]) which reflects the ability of a contrast agent to enhance the contrast increases from 2.5 $mM^{-1}\cdot s^{-1}$ to 4.1 $mM^{-1}\cdot s^{-1}$ (i.e., the enhancement of the contrast is greater) when the concentration range is reduced from [0−5 mM] to [0−0.4 mM]. These r_1 values are of the same order than the one measured previously for Au@$DTDTPA_{150}$ (r_1 = 3.9 $mM^{-1}\cdot s^{-1}$)[26] but for a gold concentration of 0.5 mg.mL^{-1} which is too weak for X-ray imaging.

The in vitro imaging experiments have shown that Au@ DTDTPA-Gd nanoparticles exert a contrast enhancement for imaging techniques which are among the most widely used for clinical diagnosis. The enhancement for CT imaging is observed for lower gold concentration (10 mg·mL^{-1}) than the concentration applied in previous works (up to 270 mg·mL^{-1}). In vivo experiments were however required to confirm the great potential of these particles for dual modality imaging. Whatever the imaging techniques, images were recorded by applying the parameters defined for the phantoms before and after intravenous injection of 300 μL (for mice) and between 0.6 and 1.8 mL (for rats) of the Au@DTDTPA-Gd_{50} colloid (gold content: 10 mg·mL^{-1}, [Gd] = 5 mM in 150 mM NaCl hepes buffered solution at pH 7.4). It must be pointed out that no trouble and no undesirable side effect were observed while the contrast agents were administrated and during at least 6 weeks following

(33) Kobayashi, H.; Kawamoto, S.; Bernardo, M.; Brechbiel, M. W.; Knopp, M. V.; Choyke, P. L. *J. Controlled Release* **2006**, *111*, 343–351.

Table 1. Gold Concentrations in Samples 1 to 8[a]

	1	2	3	4	5	6	7	8
$[Au]_{exp}$ (mg of Au $\cdot mL^{-1}$)	10.00	7.00	5.60	2.80	1.40	0.56	0.14	5.60
$[Au]_{meas}$ (mg of Au $\cdot mL^{-1}$)	9.19 ± 0.07	6.53 ± 0.16	4.67 ± 0.06	2.59 ± 0.04	1.27 ± 0.05	0.28 ± 0.06	0.14 ± 0.04	5.35 ± 0.05

[a] $[Au]_{exp}$: expected concentrations; $[Au]_{meas}$: gold concentration measured by SRCT technique at gold K-edge energy.

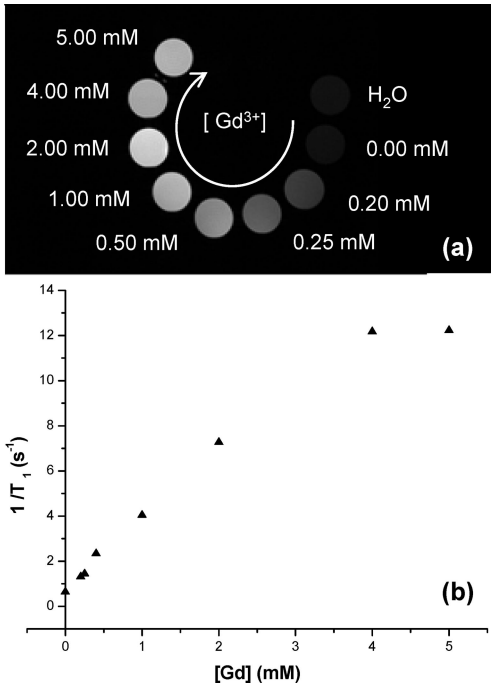

Figure 3. (a) T_1-weighted magnetic resonance images of water as negative control (H_2O) and of aqueous colloids of Au@DTDTPA-Gd_x with increasing amount of Gd (from 0 ($x = 0$) to 5.00 mM ($x \approx 50$ per particle), [Au] = 50.7 mM). (b) Water proton longitudinal relaxation rate ($1/T_1$) of Au@DTDTPA-Gd_x as a function of increasing gadolinium concentration.

the injections. Figure 4 displays a series of transmission images of a rat submitted to two X-ray beams bracketing the gold K-edge energy (see experimental section). The examination of these images reveals the appearance of brighter zones after the nanoparticles were injected. This contrast enhancement is induced by the accumulation of gold nanoparticles in these regions. At 3 min after the injection ($t_0 + 3$ min), kidneys which were not visible before the injection ($t_0 - 2$ min) can be detected due to the accumulation of gold nanoparticles. The set of images taken at various times after injection shows obviously that particles accumulated first in the kidneys and then in the bladder before being evacuated by the urine (Figure 4a).

Despite their small diameter, the ureter and urinary tract can be delineated and the gold concentration in the ureter at $t_0 +$ 10 min amounted to 5.50 $g \cdot L^{-1}$. The determination of the concentration of gold in the rats from the images has great importance because it allows monitoring quantitatively the biodistribution of gold nanoparticles (Table 2).

The gold concentrations determined from X-ray images show that the number of gold nanoparticles in the kidneys is almost constant between $t_0 + 10$ and $t_0 + 30$ min before decreasing dramatically, since the concentration is too low to be determined at $t_0 + 45$ min. The CT images including kidneys obviously illustrate this evolution which reflects a steady-state regime of filtration up to 30 min because the gold content in kidneys does not vary while the bladder fills up. The postmortem ICP analysis of the organs of a rat sacrificed 25 min after the gold nanoparticles' intravenous injection confirmed that the gold element was essentially present in urine and kidneys (Figure 5).

The uptake in lung, liver, spleen, and heart was lower than that in kidneys (Figure 5). Whereas the accumulation of gold in kidneys results from their filtration function, the detection of gold in lung, liver, and spleen can be assigned to the presence of blood in these organs, since the gold content is almost the same as that in the heart. The absence of undesirable accumulation of nanoparticles in liver and spleen which are organs with major phagocytic cells indicates that the uptake of Au@DTDTPA-Gd_{50} by macrophages is very low. Moreover they do not aggregate because they are not blocked by the thin capillaries in the lungs. Unlike the case for larger gold nanoparticles, the coating of Au@DTDTPA-Gd nanoparticles with antibiofouling poly(ethylene glycol) is not required since they freely circulate in the blood pool without undesirable accumulation in liver and in spleen and are efficiently cleared by renal elimination. As soon as the kidneys and bladder were detected by transmission imaging, serial SRCT images were recorded. Figure 4b shows transverse slices including the right and left kidneys and a vertebral body, while Figure 4c displays a transverse slice including the bladder. Owing to the measurement method, SRCT provides images with greater contrast than transmission techniques do. As a result, the delineation of labeled zones is more evident, and the interpretation of the images is more reliable. It is particularly obvious in the case of kidneys whose gold nanoparticle accumulation is more easily monitored when images are acquired by SRCT techniques (Figures 4b) as compared with the transmission technique (Figure 4a).

Moreover the follow-up of the biodistribution of Au@DTDTPA-Gd is not restricted to a single slice since the whole organism or one of its parts can be visualized through an ordered succession of SRCT images each corresponding to a different slice. For instance, the right kidney of a rat (which is nearer to the head than the left kidney is) was entirely imaged from the head to the tail by a set of successive slices (Figure 6). The contrast induced by Au@DTDTPA-Gd is sufficiently high to accurately observe the kidney vascularization and even the thin ureter (U in Figure 6) which binds this kidney to the bladder. Unsurprisingly, the left kidney exhibits a similar structure. After injection of the same AuDTDTPA-Gd_{50} nanoparticles content as that in the case of SRCT imaging, MRI experiments on rats and mice were also carried out since the in vitro studies demonstrated the ability of AuDTDTPA-Gd to greatly enhance the MR images' contrast (Figure 7).

This study confirms that these particles can be applied as contrast agents for MRI. A striking positive contrast appears first in the kidneys and then in the bladder. As expected, the follow-up by MRI of the circulation of these particles injected in rats and in mice yielded identical results to those obtained with X-ray imaging techniques. Although the gadolinium content in AuDTDTPA-Gd_{50} is weaker than the gold content (5 mM versus 50.7 mM), the contrast induced by these particles is

(34) Hainfeld, J. F.; Slatkin, D. N.; Smilowitz, H. M. *Phys. Med. Biol.* **2004**, *49*, N309–N315.

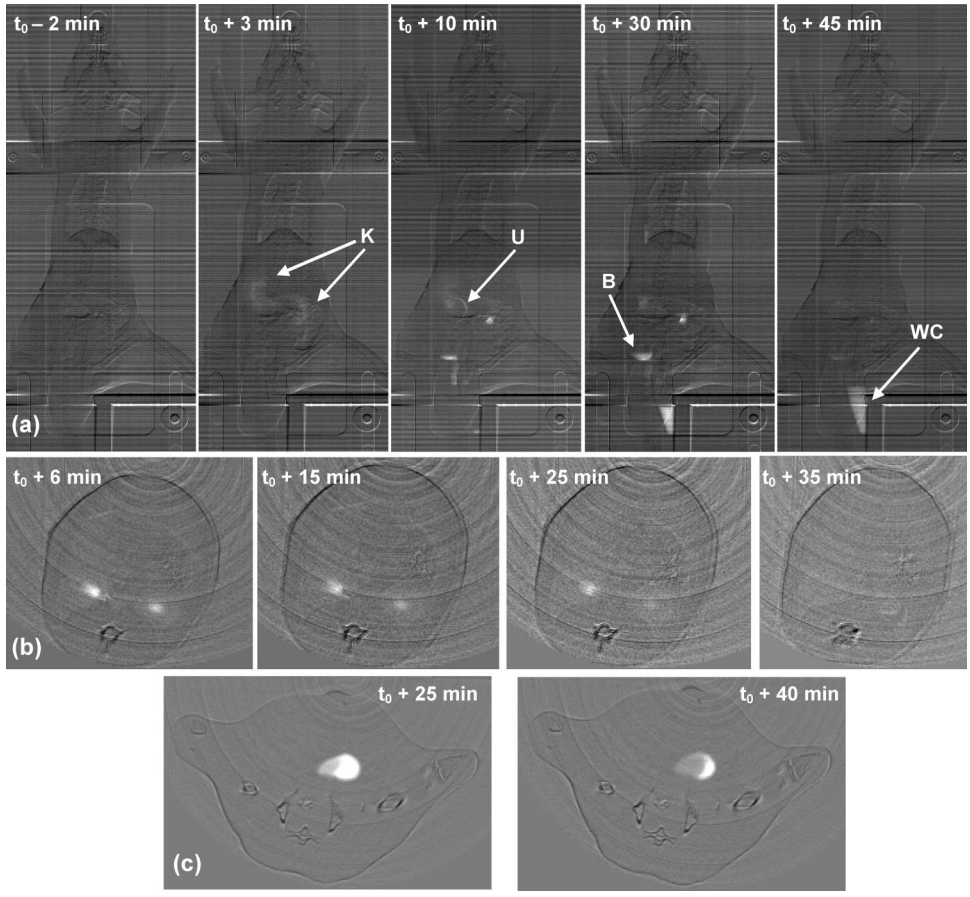

Figure 4. (a) Planar X-ray images in transmission mode of a rat before (t_0 − 2 min) and after injection of Au@DTDTPA-Gd_{50} (K for kidneys, U for ureter, B for bladder and WC for the tube collecting the urine). SRCT images of transverse slices recorded at various times after injection of Au@DTDTPA-Gd_{50} to a rat including (b) kidneys and (c) bladder (slice thickness: 1 mm).

Table 2. Gold Content at Various Times after Injection Determined by Calculation from SRCT Images (Figure 4a)

	kidney	ureter	bladder	urine
gold content at t_0 + 10 min (mg·mL^{-1})	2.59	5.50	5.77	0
gold content at t_0 + 30 min (mg·mL^{-1})	2.86	n/a	4.82	11.97

higher in the case of MRI than for SRCT imaging. At 45 min after the injection, the contrast in the kidneys is still obvious,

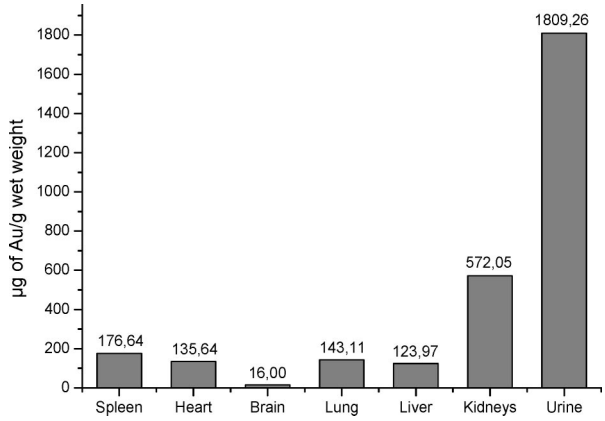

Figure 5. ICP-MS of some organs and urine of a rat which was sacrificed 25 min after the intravenous injection of Au@DTDTPA-Gd_{50}.

while kidneys are no longer observed by SRCT. Indeed MRI is more sensitive than X-ray imaging techniques, but it does not rule out the application of these particles as contrast agents for SRCT. If their use as positive contrast agents for clinical diagnosis by MRI should afford more reliable results, the SRCT which rests on the contrast generated by Au@DTDTPA-Gd could be a key element for radiotherapy. Besides their ability to enhance the image contrast, Au@DTDTPA-Gd could be applied as a radiosensitizer for radiotherapy since Hainfeld et al. demonstrated that the injection of gold nanoparticles (with a diameter of 1.9 nm but with an unknown surface composition) to tumor bearing mice led to the eradication of tumors after the mice were submitted to a X-ray beam whose dose is largely lower than the one delivered in the absence of gold particles.[34] The SRCT, which is performed with the same X-ray beam as that for the therapy, would allow imaging of diseased tissue just before irradiation. As Au@DTDTPA-Gd_{50} nanoparticles permit us to visualize zones as small as the ureter (Figure 6), SRCT images will be done in order to determine that there is a sufficient amount of gold nanoparticles and to determine with high precision the zone to be irradiated. Such an application requires a selective targeting of the diseased tissue which can be accomplished through the grafting of cRGD in the case of solid cancerous tumors.[35]

Conclusion

X-ray imaging and MRI experiments coupled to ICP analysis show that Au@DTDTPA-Gd nanoparticles can be applied as

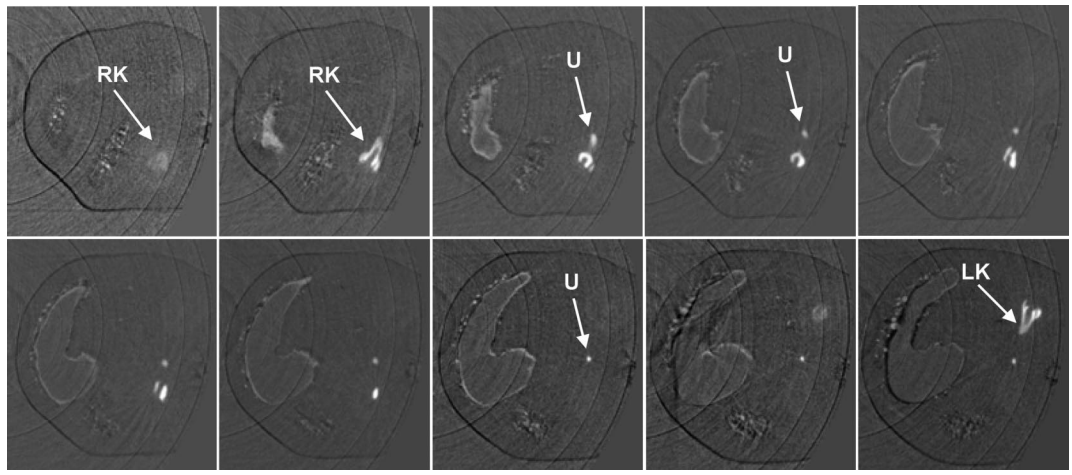

Figure 6. SRCT images of a series of successive transverse slices including right kidney (RK) of a rat from the head (top left) to the tail (right down). The images were recorded 10 min after the intravenous injection of Au@DTDTPA-Gd_{50} to a rat (RK and LK for right and left kidneys, respectively; U for ureter).

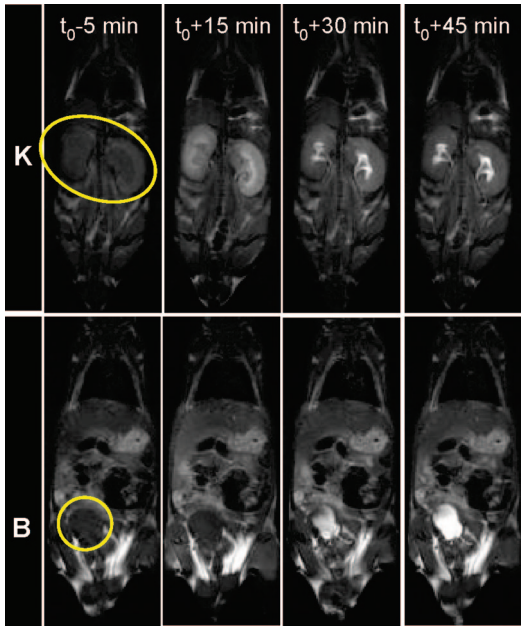

Figure 7. T_1-weighted images of a mouse 5 min before (t_0−5 min) and 15, 30, and 45 min after intravenous injection of Au@DTDTPA-Gd_{50} (K for kidneys and B for bladder).

in vivo contrast agents for both imaging techniques which are the most widely used for preclinical research. Despite the low content in gold (10 mg·mL^{-1}) and in gadolinium (5 mM), the particles were easily detected. Their ability to freely circulate in the blood pool without undesirable accumulation in the lungs, liver, and spleen, along with the fact that they can be followed up by either MRI or X-ray imaging, is very attractive for specific targeting because the accumulation would result only from the specific interaction between the biotargeting groups on the particles and the targets present in the zone of interest. Specific targeting which is required for the early detection of cancer and its treatment can be achieved by the covalent grafting of biotargeting groups on the organic multilayer of the Au@DTDTPA-Gd nanoparticles since each DTDTPA ligand possesses three COOH moieties as anchoring sites. As gold nanostructures are able to induce the destruction of cancerous cells after activation with an external physical stimulus (electromagnetic radiation in X-ray[34] and near-infrared spectral domains[36,37]), the development of nanoparticles for targeted diagnosis and therapy can therefore be envisaged with Au@DTDTPA-Gd nanoparticles.

Acknowledgment. This work was supported by the Agence Nationale de la Recherche (ANR-05-NANO-037-02).

Supporting Information Available: Conventional CT images and the complete ref 29. This material is available free of charge via the Internet at http://pubs.acs.org.

JA078176P

(35) Montet, X.; Funovics, M.; Montet-Abou, K.; Weissleder, R.; Josephson, L. *J. Med. Chem.* **2006**, *49*, 6087–6093.
(36) Loo, C.; Lowery, A.; Halas, N. J.; West, J.; Drezek, R. *Nano Lett.* **2005**, *5*, 709.
(37) Huang, X.; El-Sayed, I. H.; Qian, W.; El-Sayed, M. A. *J. Am. Chem. Soc.* **2006**, *128*, 2115.